

Effects of the Electrodes' Shape and Graphite Quality on the Arc Stability During Hydrogen Plasma Smelting Reduction of Iron Ores

Daniel Ernst,* Michael Andreas Zarl, Manuel Andreas Farkas, and Johannes Schenk

Reducing greenhouse gases (GHG), especially CO₂, is necessary to counteract climate change. The European steel industry currently corresponds to 5.7% of the total EU emissions and must therefore minimize their GHG fractions in the future. One of the most promising technologies to eliminate CO₂ emissions while directly reducing iron ore to steel in a single step is the hydrogen plasma smelting reduction. The stability of the plasma arc, which is determined by the properties and geometry of the graphite electrode, has a substantial impact on the process' economic feasibility. To study the arc stability concerning the graphite quality, tip geometry, and electrode gap, a series of experiments is conducted. The results are evaluated to create stability maps and fields to identify stable process parameters. The geometry of the graphite cathode shows the primary influence on arc stability. Tips with a flat end (standard version) offering the most unstable and a machined step on the graphite cathode providing the most stable conditions. However, an additional coating to prevent side arcing leads to the deterioration of the arc. The two graphite grades tested, with different maximum grain sizes and price classes, show no great relevance to the stability of the arc.

anthropogenic CO₂ emissions worldwide.^[4] Europe (EU28) produced 2 019 649 million tonnes of crude steel via the integrated route, blast furnace (BF)—basic oxygen furnace (BOF), which accounts for 59.1% of the total production in Europe. Worldwide, about 70% of the 1.87 billion tonnes (2020^[5]) of crude steel are produced via the BF-BOF route per year. During this established process, specific estimated emissions of 1,8 t CO₂/t steel are generated with an energy demand of 12.31 GJ tHM⁻¹ and 1.22 tCO₂ tHM⁻¹ for the blast furnace alone.^[3,6,7] To reduce or avoid these greenhouse gas emissions in steel production, the European Steel Association's members created two main technology pathways: smart carbon usage (SCU) and carbon direct avoidance (CDA). SCU consists of process integration (PI) to modify existing processes and technologies based on fossil fuel and carbon

capture and utilization (CCU) to use the emissions to produce essential chemicals.

However, CDA is focusing on developing production processes that are not producing direct CO₂ emissions because carbon carriers are left out of the process. This can be achieved with green electricity or hydrogen as a reduction agent or both.^[6,8]

1. Introduction

1.1. Current Situation of the European Steel Industry


With the European Green Deal (EGD), the European Union will become 2050 the first carbon-neutral continent. Additionally, greenhouse gas (GHG) emissions should be reduced by 55% by 2030 compared to 1990.^[1–3] With a proportion of around 7%, the iron and steel industry significantly contributes to

1.2. Hydrogen Plasma Smelting Reduction

The so-called hydrogen plasma smelting reduction (HPSR) process is one of these crucial technologies for green steelmaking in the future and is being studied by several working groups.^[9–11] The Montanuniversitaet Leoben, Austria, has been working on this research topic for more than ten years.^[12–17] With this process, iron ore fines are melted and reduced to metallic iron, leaving only steam as a by-product. A thermal transferred direct current arc is ignited between a hollow graphite electrode (HGE) and the melting pool. Gases such as hydrogen, argon, nitrogen, and iron ore fines (<150 μm) are injected through the electrode. Due to the high thermal energy of the arc, gas molecules or atoms transform in several intermediate stages until the ionized state is reached. In this final stage, the highest reduction potential occurs. Decisive for the degree of ionization, hydrogen utilization and reduction kinetics are the stability of the arc and the position of the focal spot. It has already been investigated that argon acts as a stabilizer in gas

D. Ernst, M. A. Zarl, M. A. Farkas
Area 3 - Low Carbon Energy Systems
Stahlstraße 14, A-4020 Linz, Austria
E-mail: daniel.ernst@k1-met.com

J. Schenk
Department of Metallurgy
Chair of Ferrous Metallurgy
Montanuniversitaet Leoben
8700 Leoben, Austria

 The ORCID identification number(s) for the author(s) of this article can be found under <https://doi.org/10.1002/srin.202200818>.

© 2023 The Authors. Steel Research International published by Wiley-VCH GmbH. This is an open access article under the terms of the Creative Commons Attribution License, which permits use, distribution and reproduction in any medium, provided the original work is properly cited.

DOI: 10.1002/srin.202200818

mixtures since less energy is needed to ionize the Ar atom compared to dissociation and ionization of the hydrogen molecule.^[18] In addition, the HGE's quality or geometry impacts the process.

1.3. Published Studies on Arc Stability

Farhadi et al.^[19] studied the influence of different electrode tips and diameters on electrical arc machining (EAM). For these experiments, electrode diameters of 1, 3, and 5 mm are used. Peak currents of 100, 300, and 500 A in air as dielectric were applied. A high-speed camera observed the arc plasma shapes at an interval of 1, 2, 3, 4, and 5 ms. They concluded that smaller electrode diameters result in a higher erosion rate, thus higher electrode gaps and greater plasma arc column (PAC) dimensions. Higher currents lead to higher crater diameters, electrode erosions, and PAC dimensions.

Montgomery et al.^[20] examined 1969 the effect of cathode geometry on the arc stability. Therefore, they ignited arcs between a graphite plate (anode) and a graphite cathode rod of different diameters (0.5–5 cm) and geometries. Column instability occurred for electrodes with hemispherical ends at currents higher than 400 A, where the cathode spot remains stationary, but the focal spot at the anode forms a circular motion as well as the arc column forms a cone shape. The frequency of the rotation was independent of currents between 400 and 2000 A but decreased with higher arc length and rose with increased electrode diameter. Cone-ended cathodes showed at the first moment more stable behavior, but due to graphite vaporization, the top of the cone eroded, and the arc became unstable. Hollow graphite tubes with flat ends showed a stable behavior up to 700 A. A further development was to use a cone-ended hollow cathode whereby stable behavior up to 2000 A was achievable. Here, too, after a longer burning time, the arc becomes more unstable due to the removal of the graphite material and, thus, the loss of shape. To counteract this phenomenon, cratered conical electrodes were tested. They discovered that higher crater diameters shift the critical current, where the arc becomes unstable to higher values.

To measure the arc stability, Seon and Munz^[21] used a hollow graphite cathode with a length of 279.4 mm, an outer diameter of

19.1 mm, and an inner diameter of 3.2 mm. The end of the electrode had a tip with an angle of 45°. Graphite was chosen as the anode material. The total voltage (ΔV) standard deviation was used as an arc stability indicator. They investigated that a stable arc could be achieved, at an Ar flow rate of 5 L min⁻¹ and 150 A, as long as the cathode tip remains sharp. After erosion, the voltage fluctuations exceed the limit of $\Delta V > 3$ V, and thus are considered unstable. Increasing the argon supply to 15 L min⁻¹ provided relief, and stable conditions were again achieved. These phenomena were also observed at higher currents of 300 and 400 A. It was also shown that the arc stability depends significantly more on the Ar flow rate than the initial interelectrode gap. Seon and Munz postulated the hypothesis that the Ar flow rate has the following four effects:^[21] 1) Increase in the electrical conductivity due to the removal of recondensed or vaporized graphite particles; 2) Steeper temperature gradient at the cathode based on the cooling effect and therefore higher arc root temperature; 3) Increased cooling on the arc periphery leads to higher ionization inside and ion-electron recombination outside the arc; 4) Creation of a more stable aerodynamic system.

Zarl et al.^[18] investigated the influence of gas composition, electrode gap, current levels, and the addition of iron ore to the gas stream on arc stability. For this purpose, the current and arc voltage were measured, and the arc behavior was visually evaluated with a camera system to create stability maps and fields. They discovered that the gas composition limits the realizable power input and that argon provides the most stable conditions because it serves as a stabilizer. Additionally, it was demonstrated that charging iron ore through a HGE significantly reduces stability, and the addition of hydrogen increases the voltage per millimeter electrode gap. Furthermore, higher fluctuations in current and voltage were measured at higher electrode gaps and lower applied currents. **Figure 1** shows the obtained stability fields for the varying amount of hydrogen and the introduction of iron ore into the system.

This study aimed to identify the influence of the graphite quality and different electrode tip geometries on the arc stability for the HPSR process to improve the process's economic feasibility and ensure a reliable operation in future scale-up steps.

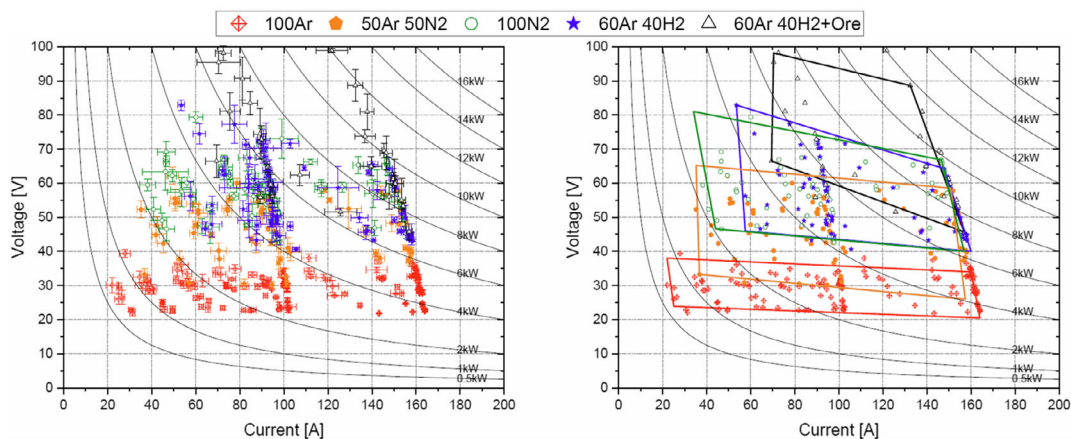


Figure 1. Arc stability fields with varying hydrogen content and the addition of iron ore through the electrode (modified). Reproduced under terms of the CC-BY license.^[18] Copyright 2020, The Authors, published by MDPI.

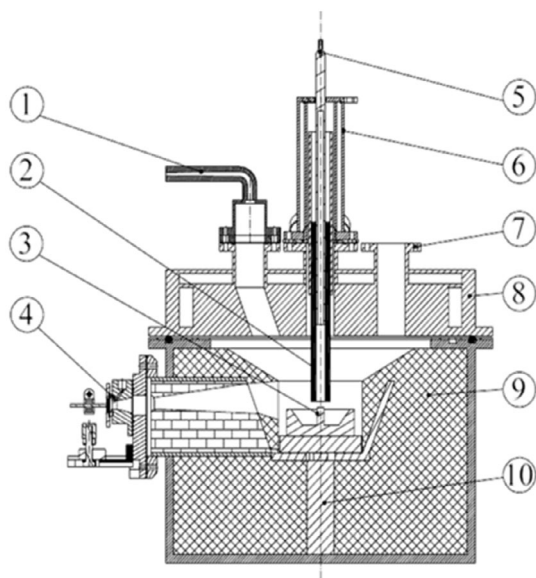


Figure 2. Reactor layout of the HPSR laboratory plant at the Montanuniversitaet in Leoben (modified). Reproduced under terms of the CC-BY license.^[18] Copyright 2020, The Authors, published by MDPI.

2. Equipment and Methods

The plasma reactor, layout see **Figure 2**, used for these experiments is located at the Chair of Ferrous Metallurgy at the Montanuniversitaet Leoben and was built in 1998 and redesigned several times over many years with improved analysis systems and measuring equipment.

2.1. Peripheral Equipment

The laboratory components consist of a DC power supply made by Messer Griesheim GmbH in Germany with a maximum output power of 16 kW at 110 V. To regulate the power input, a silicon controlled rectifier (SCR) is used and enables a seamless regulation of the electrical current. The reactor is water cooled by several circuits. Flow indicators control the cooling supply to the electrode holder (6), the reactor lid (8), and the lower vessel (9). For visual observation, a camera, “Axis-Q1775”, from Axis Communication AB, Sweden, is installed angled at one of five flange connections on the reactor lid, as shown in **Figure 3**. The gas is provided via “EL-FLOW PRESTIGE F-201C” mass flow



Figure 3. Axis-Q1775 and their attachment to the reactor lid. Reproduced under terms of the CC-BY license.^[18] Copyright 2020, The Authors, published by MDPI.

Table 1. Purity and residuals of the process gases.^[24]

Product name	Purity [%]	O ₂ [ppm]	H ₂ O [ppm]	N ₂ [ppm]
Hydrogen 5.0	≥99.999	≤2	≤5	≤3
Argon 5.0	≥99.999	≤2	≤3	≤5
Nitrogen 5.0	≥99.999	≤3	≤5	-

controllers from Bronkhorst High Tech BV, Netherlands. With these, Ar, H₂, and N₂ could be supplied for the process. They provide flows between 0 and 10 L min⁻¹ (5). The quality of the individual gases can be found in **Table 1**.

The exhaust gas treatment takes place in several stages. First, the coarse dust fraction is separated in the ABB Ltd hot gas filter “FE2”. The finer fraction is removed in the fine gas filter and then a water solution mixed with gum Arabic to decrease the wetting angle of carbon flakes is used to separate the remaining dust particles. Afterward, the gas is dehumidified via a molecular sieve, and a partial stream is passed over the mass spectrometer “GAM 200” from Pfeiffer Vacuum Technologies, Vienna. The current and voltage measurement are done by a 4-channel analog logger “HOBO UX120-006M” with a measuring interval of 1 s.

2.2. Plasma Reactor

At the laboratory facility, a DC transferred arc is ignited between the HGE (2) and an electrically conductive crucible (3), which is connected to the bottom anode (10). Depending on the experiments, refractory, graphite, or steel crucibles with an ignition pin are used. As mentioned before, a graphite disk, technical data see **Table 2**, is used in these experiments. To characterize the details of the plasma beam, optical emission spectroscopy (OES) (4) was attached to the side wall of the reactor. Five orifices are used to monitor the arc, pressure measurement, exhaust gas socket, centric HGE guiding, and lateral hydrogen injection.

2.3. Crucible and Electrode Geometries

During the preliminary stability experiments with a steel crucible as an anode, welding beads developed due to the high temperatures of the focal spot. As a result of higher current densities, the weld beads on the crucible surface are more preferred locations for the arc to burn. The experiments were performed with a graphite disk as an anode to eliminate this interference factor (see **Figure 4**).

To investigate the influence of the electrode qualities on the arc stability, two different graphite grades, GE and CGS from

Table 2. Technical data for the graphite anode and both electrodes.

Properties	Unit	Anode Grade		
		EG75	GE	CGS
Spec. el. resistivity	μΩm	8	6.57.0	13
Bulk density	g cm ⁻³	1.75	1.61.68	1.78
Compressive strength	MPa	35	2022	84
Max. grain size	mm	0.8	<2	<0.02
Ash content	%	0.1	<0.3	<0.005

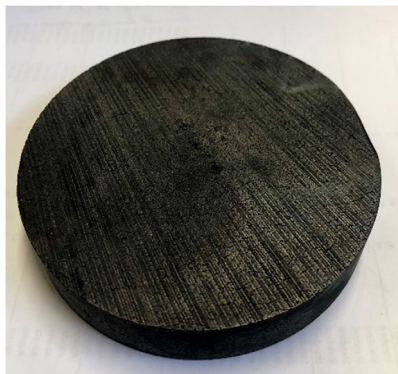


Figure 4. Ø100 × 20 mm graphite anode.

Henschke GmbH in Germany, were used, see **Table 2**. For each cathode type, three different electrode tips were fabricated, see **Figure 5**, to study the impact of the geometry. The standard version (a) consists of a flattened cylindrical tip with a 5 mm inner diameter. Type 2 (b) has a machined 20 × Ø10 mm step to reduce the cathode cross-sectional area. A 5 × 5 mm cut was made crosswise on the face to produce the last geometry (c), and a 2 mm chamfer was applied. This divided the face of the electrode into four areas. Additionally, a coating of 92% Al₂O₃, 4.6% CaO and 1% SiO₂ on the step-shaped tip was used to determine an effect on the arc stability. For this purpose, the base material was moistened with ethanol and applied to the sheath surface of the electrode tip.

2.4. Experimental Procedure

After the complete assembly of the reactor system and the connection to the cooling cycle and gas supply, an Ar purging was initiated to remove the remaining oxygen. Afterward, the cathode was moved to contact the anode via a motorized spindle drive. The power supply was activated under the physical contact of both electrodes, and an argon flow rate of 5 L min⁻¹ was applied. After the arc was visible, the cathode was raised immediately to an defined electrode gap. The desired gas composition, with a total flow rate of 5 L min⁻¹, was set and the time measurement

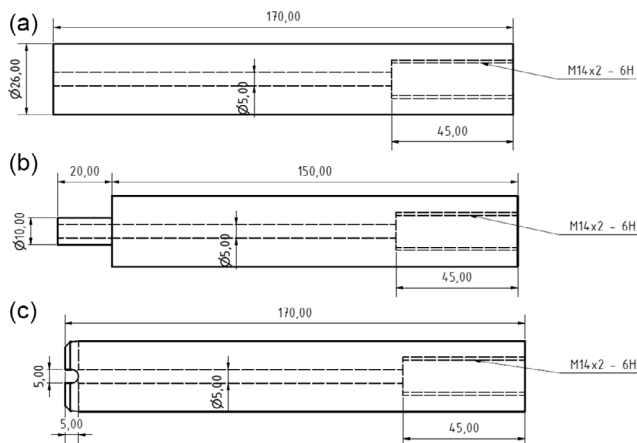


Figure 5. a–c) Used electrode geometries.

started. With a potentiometer connected to the SCR power controller, the current was steadily decreased by 5 % every 10 s until the arc extinguished. Finally, the reactor was flushed again with argon. This procedure is then carried out again for the various electrode heights, geometries, and qualities.

2.5. Evaluation Methods

The current and voltage values were measured with a 4-channel analog logger, and the arc movement was observed with the camera. As already published by Ernst et al. [22], the amount of hydrogen in the plasma gas is one determining factor for the oxygen removal rate in the HPSR process. Therefore, the experiments focused on those with an increased hydrogen content (40%) in order to be able to investigate various influences on the stability under these process conditions. This gas composition was chosen because experience has shown that stable conditions can still be achieved at 40% H₂, and at higher contents this is no longer guaranteed for the laboratory reactor. The plasma furnace works with a current-controlled system, whereby the arc voltage is adjusted depending on the arc length and the gas composition. The maximum current available for the process can be limited via the regulation of the SCR controller. The HOBO UX120 data logger measures a step-shaped current curve through the steady decrease, as shown in **Figure 6**.

After the arc ignition under pure argon, the desired electrode gap is adjusted (I). This causes a slight current drop because the voltage increases due to the higher electrical resistance. At (II), 40% hydrogen was added, and a further voltage increase occurred. Then, the potentiometer of the SCR controller was gradually reduced by 5% every 10 s. The maximum available current hardly changes between 100% and 90% due to the principle of phase angle control (PAC).

The SCR unit is turned on at a specific phase angle of the AC power supply (sinusoidal oscillation). The power is controlled by advancing or delaying the timing of the SCR turn on in each half cycle. **Figure 7** shows a PAC at a power output of 50%.

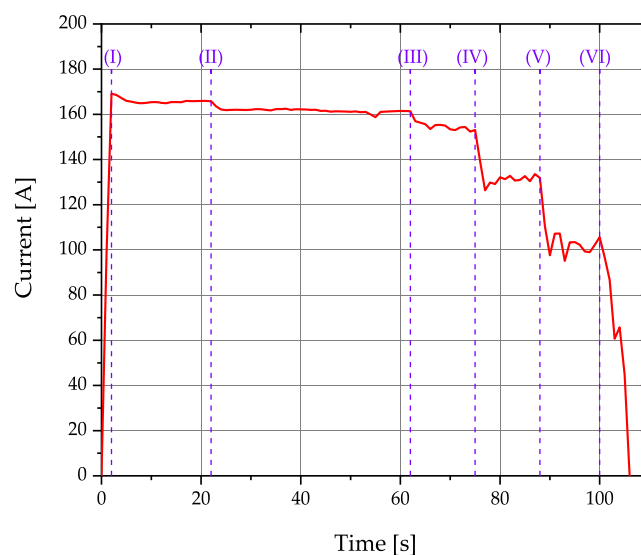


Figure 6. Current progression with the different areas due to the SCR regulation.

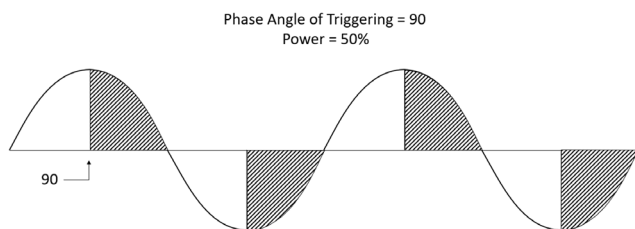


Figure 7. Phase angle control for a power output of 50%.

The further the time for the SCR is delayed, the larger the truncated area under the curve and the lower the output power.^[23]

From (III), potentiometer position 85%, the current is noticeably reduced, kept at a more or less constant value for at least 10 s and then reduced by a further 5%, (IV) and (V). A subsequent reduction of the current (VI) finally led to extinguishing the arc.

The visual analysis showed that adding hydrogen to the argon plasma leads to an eccentric shift of the arc position, as shown in **Figure 8**. During the evaluation of these current–voltage curves, the behavior of the arc appears very stable. However, since eccentric burning of the arc should be avoided in the process, the evaluation consists of two steps. The video footage of the experiments was evaluated first. When the arc moved to the outer area of the graphite plate and side arcing occurred, the behavior was considered unstable, and an analysis of the current–voltage progression, step two, was not performed. If the arc remains in the centric area, a subsequent analysis of the power input was carried out. The arc position and

Table 3. Arc stability map for the CGS graphite quality and $20 \times \varnothing 10$ mm step on the electrode tip.

Ar/H ₂ 60%/40% CGS and Step	Level SCR power controller [%]						
	100	95	90	85	80	75	70
Electrode gap [cm]							
2.0	Green	Green	Green	Green	Green	Yellow	Red
2.5	Green	Green	Green	Green	Green	Red	Red
3.0	Green	Green	Yellow	Yellow	Red	Red	Red
3.5	Green	Green	Green	Red	Red	Red	Red
4.0	Red	Red	Red	Red	Red	Red	Red

characteristics for each material, tip geometry, and electrode gap were examined and divided into stable, fluctuating, and unstable categories. Using this classification, arc stability maps (e.g., **Table 3**) could be generated for both graphite materials and electrode tips.

The arc stability maps consist of three different colors: 1) Green: Stable arc that burns within the defined range or at its boundary and shows no fluctuations. 2) Orange: The plasma arc is located within or on the boundary of the defined area but changes its position abruptly (fluctuation) or shows chaotic movement. 3) Red: Unstable behavior because the arc is no longer located in the specified region.

Figure 9 shows examples of the different positions, which can be classified into the categories a) stable, b) fluctuating/chaotic

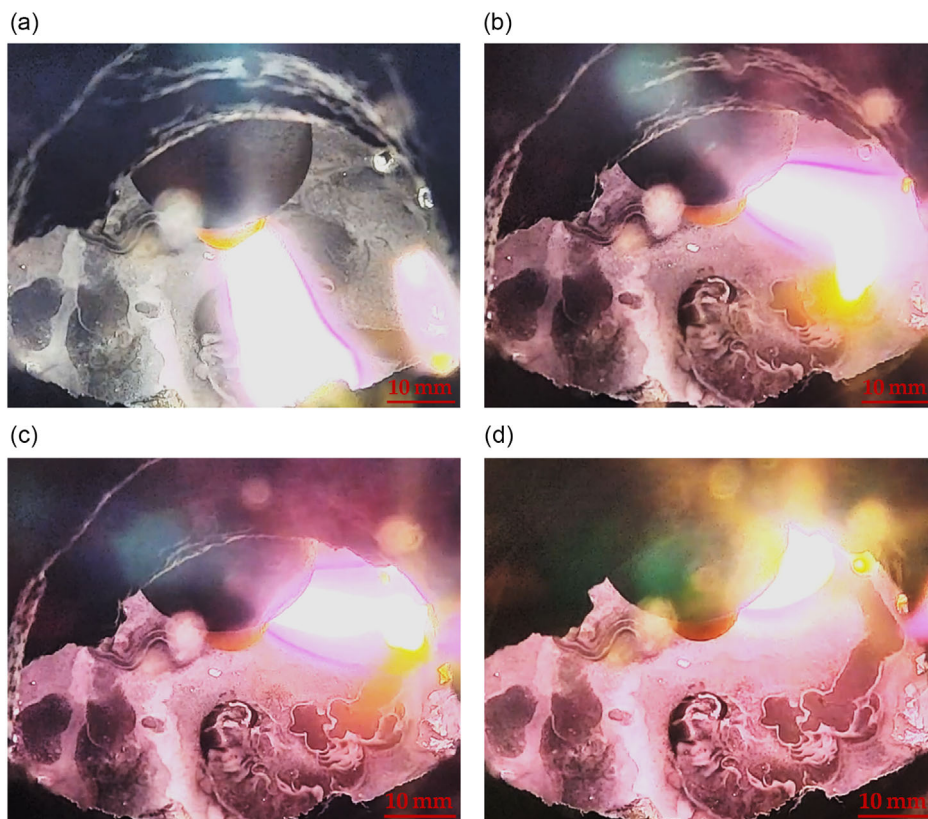


Figure 8. Shifting of the arc when hydrogen is added into the reaction zone (a) to (d).

and c) unstable. The dotted circle represents the defined area where the arc is considered stable when it is within or at its limit.

This classification into three arc characteristics makes it possible to determine the unstable process parameters, which can then be excluded for further evaluation. The second step uses the voltage and current measurement to create arc stability fields. These consist of a voltage over current diagram with the values of the stable or fluctuating measuring points, see **Figure 10**.

The stability field aims to show the voltage and current range for stable arc performance at certain electrode quality and tip geometry. The larger the area of the stable field, the more extensive the range in which the arc has a stable behavior. If the field extends in a wide span along the X-axis, the plasma beam maintains even at low currents and, therefore, low power. If, on the other hand, the field covers a wide range in the Y-axis, and high arc length and power inputs are achievable.

3. Design of Experiments

A total of eight experiment series, **Table 4**, were carried out to investigate the arc stability depending on the graphite quality, tip geometry, and electrode gap. Each series started at a distance between the cathode and the anode of 20 mm, followed by a steadily decreased current. Afterward, the gap was increased by 5 mm for the subsequent trial. This was done up to a maximum of 40 mm.

4. Results and Discussion

4.1. Stability Maps

With the evaluation of the video footage and the already described classification into three arc characteristics, it is possible to create stability maps for each electrode quality and tip geometry, see **Table 5**.

Independent of the graphite quality, a stable operation with the standard cylindrical tip is impossible, even with the smallest electrode gap of 2 cm. This is attributable to the fact that the arc, cathode spot, consistently discharges at the edge of the tip. As a result, the arc is already shifted from the center of the crucible by the radius of the electrode tip, see **Figure 11**.

The machined $20 \times \varnothing 10$ mm step on the tip solves this issue due to a decrease in the electrode diameter by 61.5%. This behavior is also reflected in the stability map, where stable conditions up to an electrode gap of 3.5 cm and an SCR level of 90% were

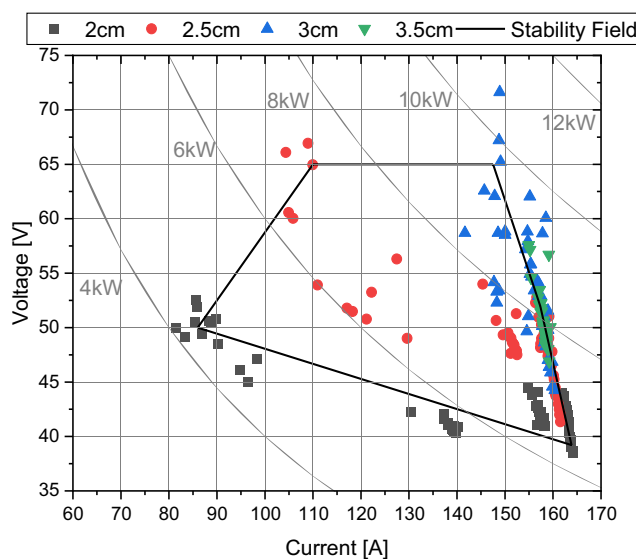


Figure 10. Stability field for the CGS quality with a machined step on the electrode tip.

Table 4. Experimental plan.

Experiment number	Cathode Grade [-]	Tip Geometry [-]	Electrode Gap [cm]	Hydrogen content [%]	Potentiometer [%]
N.1-1	CGS	Standard	2.0–4.0	40	75–100
N.1-2	CGS	Step	2.0–4.0	40	75–100
N.1-3	CGS	Step coated	2.0–4.0	40	70–100
N.1-4	CGS	Slotted	2.0–4.0	40	75–100
N.2-1	GE	Standard	2.0–4.0	40	75–100
N.2-2	GE	Step	2.0–4.0	40	75–100
N.2-3	GE	Step coated	2.0–4.0	40	75–100
N.2-4	GE	Slotted	2.0–4.0	40	80–100

achieved. An alumina coating was used to avoid side arcing at the sheath surface of the electrode tip. At the beginning of the test series, a gap of 2 cm, results are obtained identical to those without coating. With progressing erosion of the electrode tip, the coating influences the arc stability negatively, whereby a stable behavior only up to an electrode distance of 3 cm was attainable. The slotted version of the electrode also improved the behavior

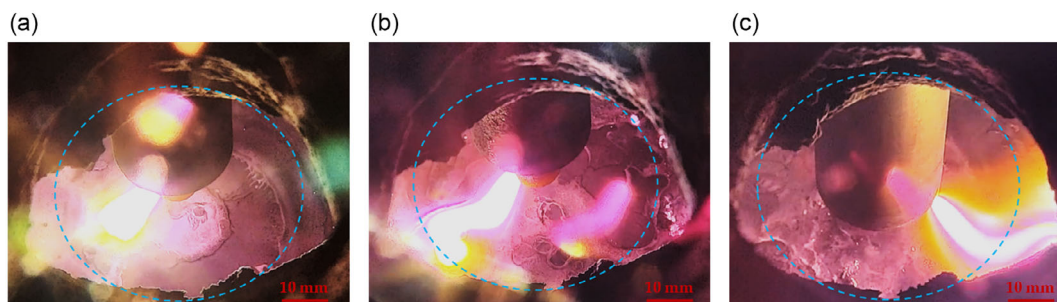
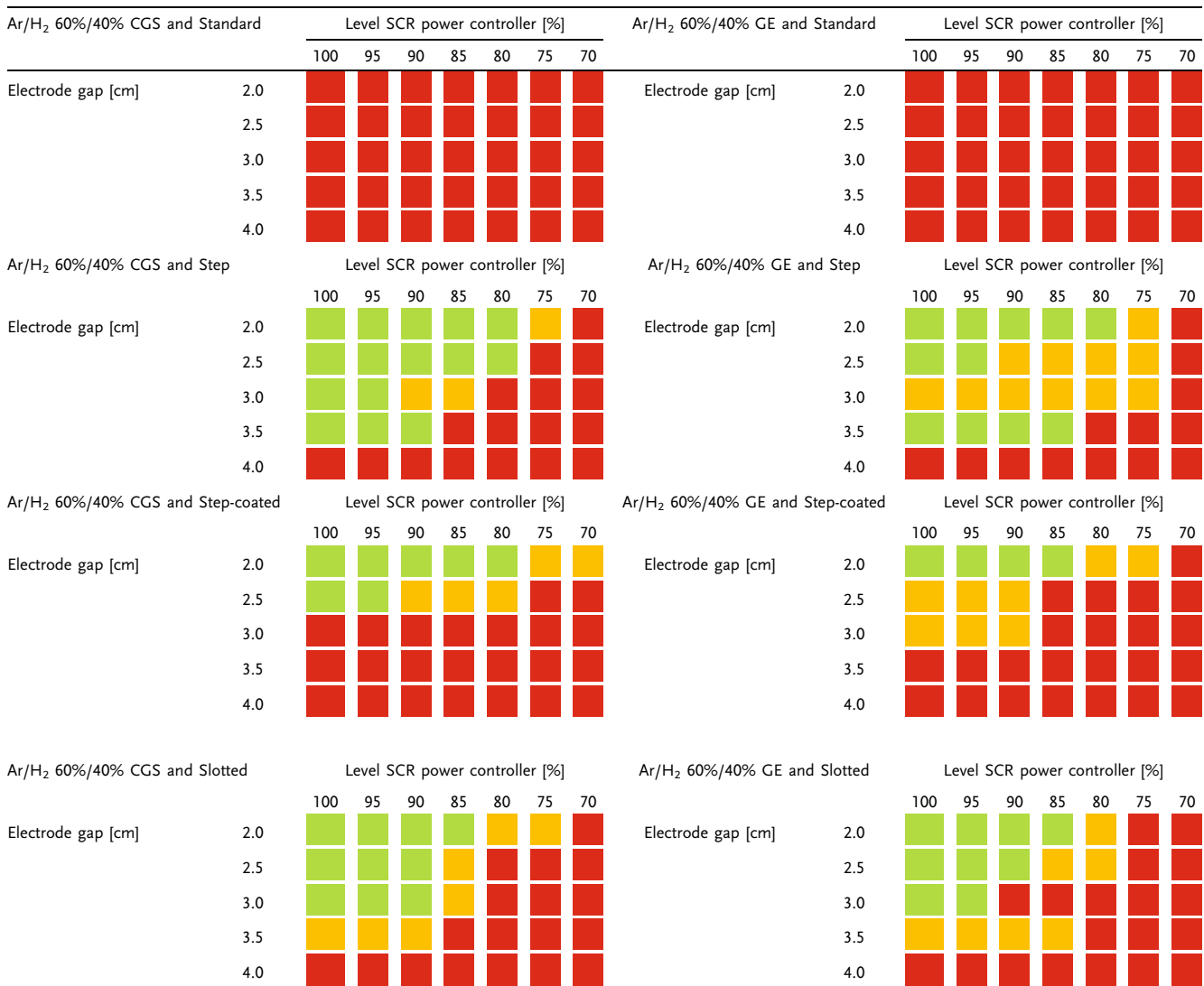


Figure 9. Plasma arc for a) stable, b) fluctuating/chaotic, and c) unstable characteristic.

Table 5. Stability maps.



compared to the standard tip. Unfortunately, the arc shows more chaotic performance at higher electrode gaps than the step shape.

Nevertheless, electrode distances up to 35 mm were reachable. The quality of the graphite electrode does not significantly affect the plasma beam's stability. With the cheaper GE-Quality, max. grain size <2 mm, higher electrode gaps, and lower SCR levels were achieved, but the tip geometry has a much more significant role in the stability of plasmas.

4.2. Stability Fields

Stability maps were used to identify stable and fluctuating process phases, whose process data were then used for the subsequent evaluation to create stability fields, see **Figure 12** for both graphite grades.

With a gas composition of 40% hydrogen and 60% argon, a total gas flow rate of 5 L min⁻¹, electrode gaps between 20

and 35 mm, and power inputs between 4 and 9.8 kW were achievable for a stable operation. It can be seen that the largest area of stability could be achieved with the graphite grade CGS and the slotted electrode tip followed by the step shape. However, the slight difference is compensated because more chaotic behavior occurred with the slotted electrode than with the stepped electrode. Following the stability maps, the step-coated shape shows the worst performance. Between the different graphite grades, it is noticeable that the GE quality does not reach as high voltage levels as the finer-grained one. This phenomenon can be partly attributed to the difference in the specific electrical resistivity, as shown in **Table 2**. Due to the much more refined grains of the CGS grade, <20 μm, there are significantly more grain boundaries within the electrode. These subsequently lead to higher electrical resistances, thus, to a higher voltage drop according to Ohm's law. The GE grade also shows a vast stability range with a step as a tip, and the coating also shows less stable areas.

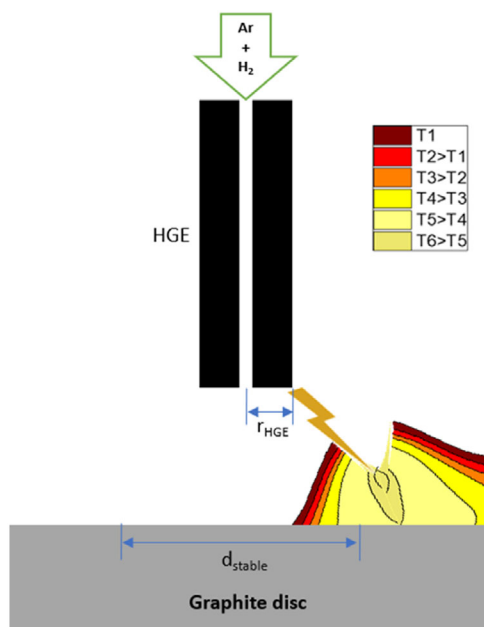


Figure 11. The shift of the cathode spot with the standard electrode geometry.

4.3. Statistical Analysis

The MODDE 13 Pro application from Sartorius AG in Germany was used to evaluate the experiment further and examine how the current and voltage depended on the SCR-Level and electrode gap. For this aim, the output was defined as responses and the variable process parameters as factors, see **Table 6**. The general settings must be chosen, including the specific factors type, range, and

precision. In case of a significant deviation, outlier experiment responses were not included in the analysis. The response distribution's shape is verified by MODDE 13 Pro, which may also apply a transformation if required. The significant coefficients of each individual response are then determined, and all unnecessary terms are eliminated. Acronyms used in the illustrations are defined in **Table 7**. The dashed lines indicate both the upper (U. conf. int) and lower (L. conf. int) confidence interval in the graphs.

The results of this analysis show the trend of the maximum current via the SCR controller level, **Figure 13**. Here too, the principle of the phase angle control, that the current keeps nearly constant between 100% and 90%, is evident. According to the figure, a slight increase is visible, but this is only due to the fitted model of MODDE 13 Pro. A closer examination of this area shows, however, that the area has a linear progression.

Figure 14 shows that the voltage behaves in the opposite manner. Due to the reduction in the current and therefore energy input, fewer atomic species are converted into the ionized state. This results in a higher electrical resistance over the entire plasma arc, thus leading to a higher voltage drop.

A similar phenomenon occurs when the electrode gap and therefore the arc length is raised. Due to the forced enlargement of the arc, the distance the charged particles have to overcome becomes longer and the electrical resistance increases. According to Ohm's law, this results in a higher voltage at constant current input, as illustrated in **Figure 15**. With 40% hydrogen and 60% argon in the plasma gas, an average voltage increase of around 8.7 V per centimeter was achieved.

With the help of these two results, a respective voltage range can be determined as a function of the SCR controller and the electrode gap, as shown in **Figure 16a**. These results, combined with the stability maps, allow defined voltage ranges to be set depending on the SCR controller as well as the electrode spacing for stable arc behavior, as shown in **Figure 16b**. The red dots represent the

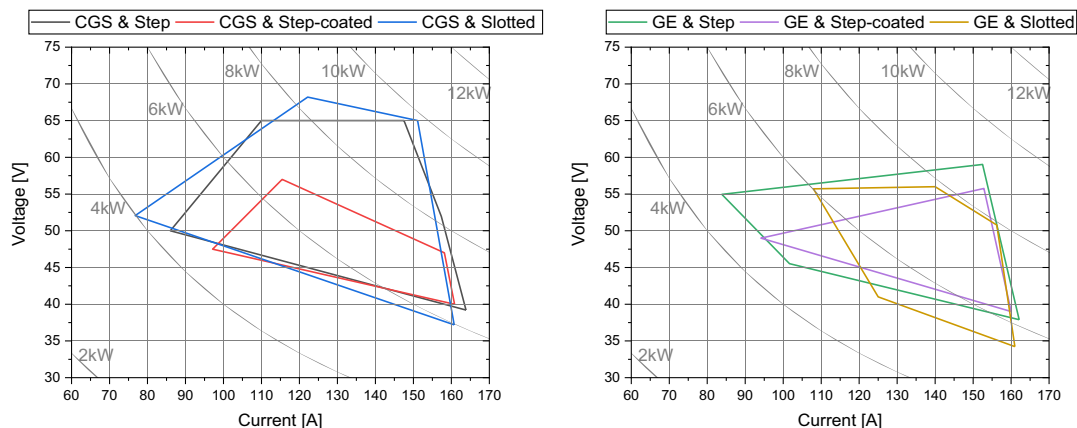


Figure 12. Stability field for the CGS (left) and GE (right) quality with different electrodetips.

Table 6. Factors and responses for the statistical analysis in MODDE® 13 pro.

Factors				Responses	
Graphite Quality [-]	Electrode Tip [-]	Level SCR Controller [%]	Electrode gap [cm]	Current [A]	Voltage [V]

Table 7. Acronyms of the statistical analysis.^[22]

Acronym	Meaning
N	Number of valid experiments responses
R2	Coefficient of determination
RSD	Residual standard deviation
DF	Number of degrees of freedom
Q2	Percent of the variation of the response predicted by the model
Interval	Confidence interval

stable areas from the stability map, resulting in an unsteady area highlighted in gray, which should be avoided for reliable operation.

Figure 17 shows that the effect of the electrode quality and the geometry of the graphite tip has only a small influence. It results

in a maximum voltage deviation of just 2.2 V and, according to the above analysis, corresponds to a difference in electrode gap of just 2.5 mm. Because of this low value, it cannot be ruled out that these voltage differences are due to inaccuracy in setting the electrode height, making the influence of the graphite material and the electrode tip on the voltage level negligible.

5. Conclusion and Outlook

5.1. Stability Maps

1) The stability maps show that the standard cylindrical tip leads to an instable plasma arc behavior even with smallest electrode gaps due to the fact that the arc, which mostly emerges at edges as a result of higher current densities, is already shifted by the electrode radius from the center of the graphite plate. 2) A

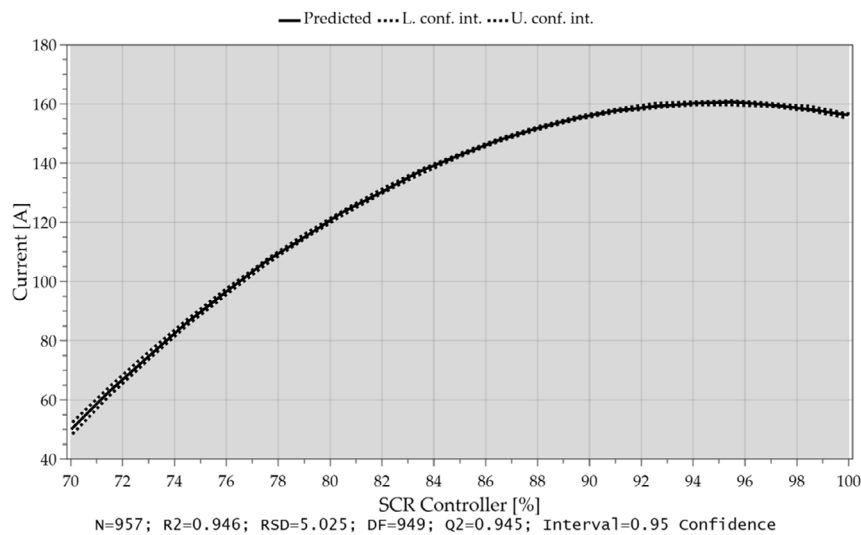


Figure 13. Amperage depending on the level of the SCR controller.

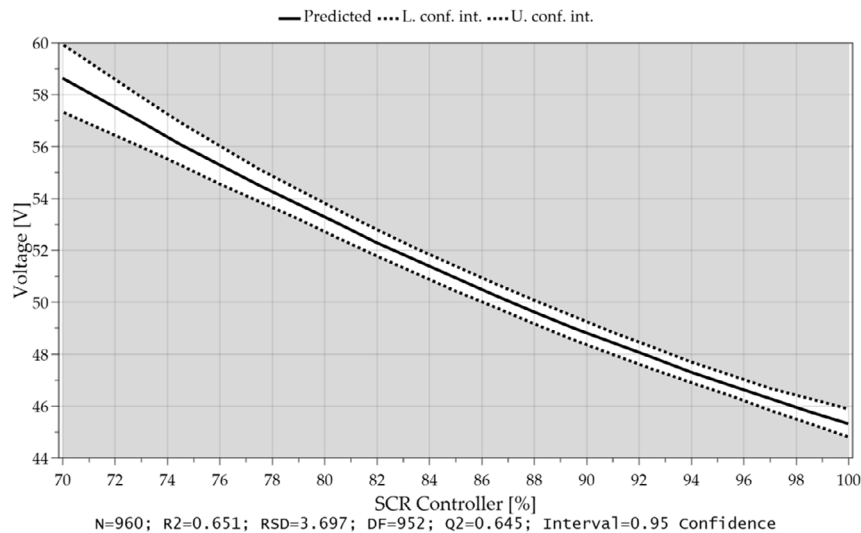


Figure 14. Voltage as a function on the SCR level.

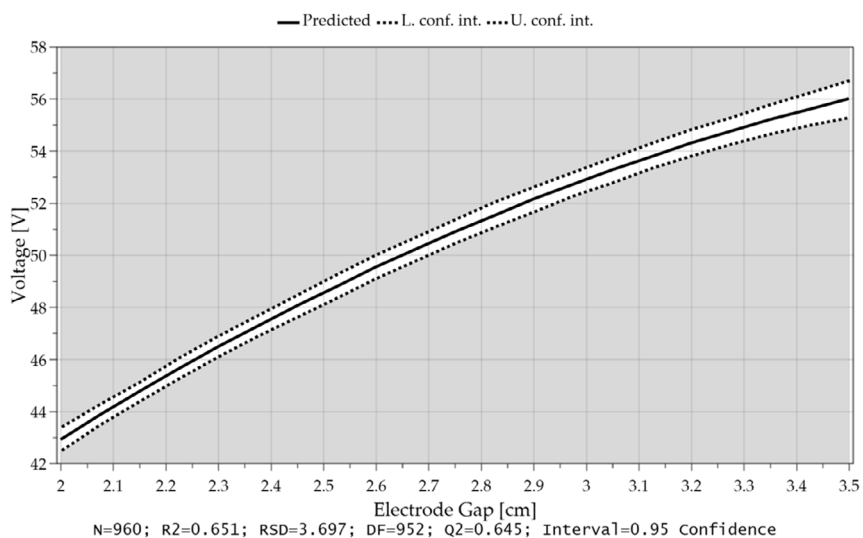


Figure 15. Voltage over electrode gap at 40% H₂ and 60% Ar in the plasma gas.

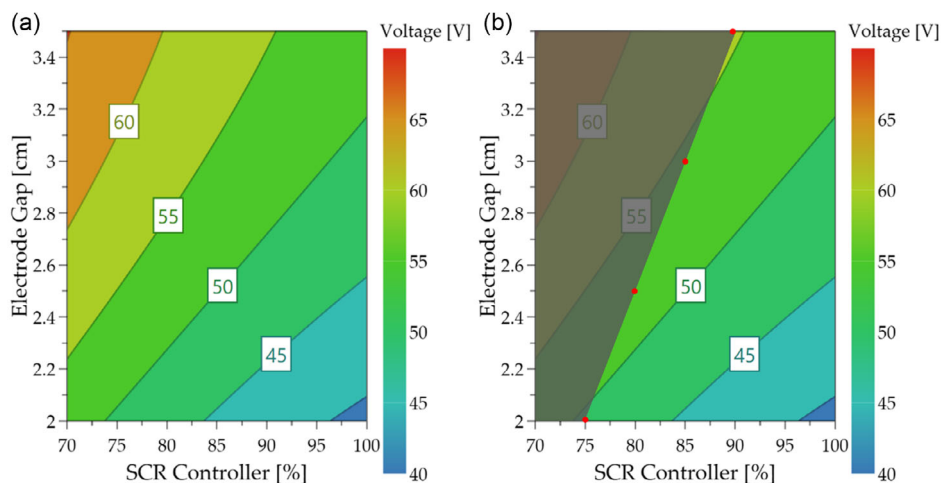


Figure 16. a) Dependence of the voltage drop and b) the combination with the stability map for the CGS quality and stepped electrode tip.

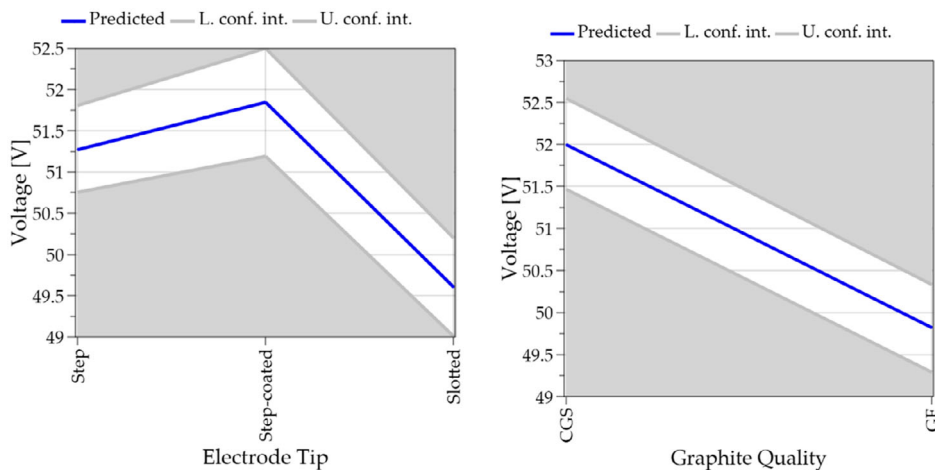


Figure 17. Influence of electrode geometry (left) and graphite quality (right) on voltage drop.

machined step as electrode tip could significantly improve stability by reducing the cross-sectional area and the arc burned more centrally. 3) The coating used had a negative effect on stability after erosion of the tip. 4) The division of the cross-sectional area into four sections by incisions of the electrode tip showed better performance than the standard or the coated version, but more chaotic behavior at higher electrode gaps appeared. 5) The stability of the plasma beam is not considerably influenced by the graphite electrode's quality. Higher electrode gaps or lower SCR levels were occasionally attained with the less expensive GE-Quality, max. grain size 2 mm; however, the tip shape plays a far larger effect in the stability of plasma arcs.

5.2. Stability Fields

1) With the slotted electrode tip and graphite grade CGS, the largest area of stability could be attained. Unfortunately, the arc's behavior was more chaotic than the step-shaped tip. 2) The step-coated design performs most poorly, as already determined in the stability maps. 3) The finer graphite quality, CGS has more grain boundaries within the electrode and therefore a higher electrical resistivity than the GE grade, which results in the GE quality not reaching as high voltage values as the finer one. 4) In conclusion, regardless of graphite quality, the stepped shape electrode tip showed the most promising behavior for stable arc conditions in the HPSR process.

5.3. Statistical Analysis

1) The dependence of current and voltage on the SCR level and electrode gap was calculated with the statistical program MODDE 13 Pro. This evaluation shows that an SCR level of 75% corresponds to an applied current of 90 A. This represents the minimum current required to produce a stable arc at an electrode gap of 2.5 cm. At higher distances between cathode and anode, higher currents are necessary and a minimum of 148 A at 3.5 cm is required. 2) The voltage drop in the arc zone depends on the one hand on the injected plasma gas composition and on the other hand on the electrode gap. At 40% hydrogen and 60% argon, a voltage drop of 8.7 V per centimeter was determined. 3) The graphite tip's geometry and electrode quality have very small impact on the voltage drop in the arc zone. The maximum difference of 2.2 V corresponds to an electrode gap of 2.5 mm and can be attributed to the inaccurate setting of the electrode gaps.

5.4. Comparison with Already Published Research

1) Montgomery et al.^[20] determined an improved arc behavior with a cone ended hollow electrode compared with flat ends. Our experiments show the same results due to the fact that the cathode spot moves further into the center of the HGE through a conical or stepped shape tip. 2) In comparison with the stability maps obtained by Zarl et al.^[18] for a plasma gas composition of 40% hydrogen and 60% argon, it is noticeable that stable behavior was achieved up to electrode gaps of 4.5 cm with a slightly sharpened graphite electrode and a steel crucible. These differences can be attributed to the melting behavior of the steel

crucible. As mentioned in Section 2.3, higher current densities in weld seams on the crucible's surface make them more favorable spots for the arc to ignite. Studies have also shown that, with sufficient power input, a certain size of molten bath also has a positive effect on stability and more or less traps the arc in the middle of the pool. Although this influence of the crucible has a positive effect on the stability, it was purposely eliminated in our investigations in order to study the pure influence of the cathode material and electrode geometry. 3) Zarl et al.^[15] postulated that with higher voltage level, low current values are not reachable. This is also reflected in these experiments. It is apparent because in the stability fields, the lower field frame moves toward higher voltages at low current values (from the lower right to the upper left). Both in their and our trials, the arc fluctuated more strongly at wider electrode distances, thus high voltage values, as well as at lower current densities. The obtained stability field for 40% H₂ and 60% Ar by Zarl is located in the power range between 3 and 9.5 kW and therefore agrees well with these results. Also the voltage variation per centimeter of arc height at 40% hydrogen and 60% argon from 6.2 to 10.3 V cm⁻¹ is in good agreement with the calculated 8.7 V cm⁻¹.

5.5. Outlook

For further experiments in the subject area, the erosion rate difference of both graphite grades should be investigated. On the one hand, the pure losses due to the evaporation of graphite, but also on the other hand during the melting and reduction of iron ore due to the influence of the heterogeneous shift reaction. Furthermore, a plasma stabilizer should be designed and built to additionally stabilize the arc in order to achieve higher electrode distances and thus higher power input.

Acknowledgements

The authors gratefully acknowledge the SuSteel project's funding by The Austrian Research Promotion Agency (FFG) and the funding support of K1-MET GmbH metallurgical competence center. The K1-MET competence center's research program is supported by COMET (Competence Center for Excellent Technologies) and the Austrian program for competence centers. The Federal Ministry funds COMET for Climate Action, Environment, Energy, Mobility, Innovation and Technology, the Federal Ministry for Digital and Economic Affairs, the provinces of Upper Austria, Tyrol, and Styria, and the Styrian Business Promotion Agency (SFG).

Conflict of Interest

The authors declare no conflict of interest.

Author Contributions

Conceptualization, D.E. and J.S.; methodology, D.E. and M.A.Z.; validation, D.E.; formal analysis, D.E.; investigation, D.E. and M.A.F.; resources, D.E.; data curation, D.E.; writing—original draft preparation, D.E.; writing—review and editing, J.S. and M.A.Z.; visualization, D.E.; supervision, J.S.; project administration, J.S.; funding acquisition, J.S. All authors have read and agreed to the published version of the manuscript.

Data Availability Statement

The data that support the findings of this study are available from the corresponding author upon reasonable request.

Keywords

arc stability, electrode geometry, graphite, hydrogen plasma smelting reduction, hydrogen reduction, iron ore, plasma

Received: October 24, 2022

Revised: January 30, 2023

Published online:

-
- [1] K. Hainsch, K. Löffler, T. Burandt, H. Auer, P. C. del Granado, P. Pisciella, S. Zwickl-Bernhard, *Energy* **2022**, 239, 122067.
- [2] R. Chauvy, G. Weireld, *Energy Technol.* **2020**, 8, 2000627.
- [3] J. Rieger, V. Colla, I. Matino, T. A. Branca, G. Stubbe, A. Panizza, C. Brondi, M. Falsafi, J. Hage, X. Wang, B. Voraberger, T. Fenzl, V. Masaguer, E. L. Faraci, L. di Sante, F. Cirilli, F. Loose, C. Thaler, A. Soto, P. Frittella, G. Foglio, C. di Cecca, M. Tellaroli, M. Corbella, M. Guzzon, E. Malfa, A. Morillon, D. Algermissen, K. Peters, D. Snaet, *Metals* **2021**, 11, 1202.
- [4] L. Holappa, *Metals* **2020**, 10, 1117.
- [5] World Steel Association AISBL, **2021** World Steel in Figures, <https://worldsteel.org/wp-content/uploads/2021-World-Steel-in-Figures.pdf>, (accessed on February 2022).
- [6] M. Draxler, J. Schenk, T. Bürgler, A. Sormann, *Berg Huettenmaenn Monatsh* **2020**, 165, 221.
- [7] H. Suopajärvi, K. Umeki, E. Mousa, A. Hedayati, H. Romar, A. Kemppainen, C. Wang, A. Phounglamcheik, S. Tuomikoski, N. Norberg, A. Andefors, M. Öhman, U. Lassi, T. Fabritius, *Appl. Energy* **2018**, 213, 384.
- [8] Eurofer The European Steel Association, Low Carbon Roadmap: Pathways to a CO₂-Neutral European Steel Industry, **2019**, <https://www.eurofer.eu/assets/Uploads/EUROFER-Low-Carbon-Roadmap-Pathways-to-a-CO2-neutral-European-Steel-Industry.pdf>.
- [9] P. R. Behera, B. Bhoi, R. K. Paramguru, P. S. Mukherjee, B. K. Mishra, *Metall. Mater. Trans. B* **2019**, 50, 262.
- [10] I. R. Souza Filho, Y. Ma, M. Kulse, D. Ponge, B. Gault, H. Springer, D. Raabe, *Acta Mater.* **2021**, 213, 116971.
- [11] H. Pauna, D. Ernst, M. Zarl, M. Aula, J. Schenk, M. Huttula, T. Fabritius, *J. Clean. Prod.* **2022**, 372, 133755.
- [12] A. Sormann, Dissertation, Montanuniversität Leoben, **1992**.
- [13] E. Bäck, Dissertation, Montanuniversität Leoben, **1998**.
- [14] J. F. Plaul, Dissertation, Montanuniversität Leoben, **2005**.
- [15] K. Badr, Dissertation, Montanuniversität Leoben, **2007**.
- [16] M. N. Seftejani, Dissertation, Montanuniversität Leoben, **2020**.
- [17] M. A. Zarl, Dissertation, Montanuniversität Leoben, **2021**.
- [18] M. A. Zarl, M. A. Farkas, J. Schenk, *Metals* **2020**, 10, 1394.
- [19] A. Farhadi, Y. Zhu, L. Gu, W. Zhao, *Proc. CIRP* **2018**, 68, 215.
- [20] R. W. Montgomery, C. M. H. Sharp, *J. Phys. D: Appl. Phys.* **1969**, 2, 1345.
- [21] H. Seon, R. J. Munz, *Can. J. Chem. Eng.* **2001**, 79, 626.
- [22] D. Ernst, M. A. Zarl, J. Cejka, J. Schenk, *Materials* **2022**, 15.
- [23] Tempco Electric Heater Corporation, SCR Power Controllers: Introduction to Silicon Controlled Rectifier (SCR) Power Controllers, (accessed: May 2022).
- [24] M. A. Zarl, D. Ernst, J. Cejka, J. Schenk, *Materials* **2022**, 15.